AWARD NUMBER: W81XWH-18-1-0628

TITLE: Longitudinal analysis of disease-site activities impairing wound healing in epidermolysis bullosa and development of therapeutic strategies

PRINCIPAL INVESTIGATOR: Dr. Olga Igoucheva, Ph.D.

CONTRACTING ORGANIZATION: Thomas Jefferson University
Philadelphia, PA 19107

REPORT DATE: September 2019

TYPE OF REPORT: Annual

PREPARED FOR: U.S. Army Medical Research and Materiel Command
Fort Detrick, Maryland 21702-5012

REPORT DOCUMENTATION PAGE

Form Approved
OMB No. 0704-0188

1. REPORT DATE	2. REPORT TYPE	3. DATES COVERED
September 2019	Annual	1 Sep 2018 – 31 Aug 2019

4. TITLE AND SUBTITLE

Longitudinal analysis of disease-site activities impairing wound healing in epidermolysis bullosa and development of therapeutic strategies

5a. CONTRACT NUMBER

5b. GRANT NUMBER
W81XWH-18-1-0628

5c. PROGRAM ELEMENT NUMBER

6. AUTHOR(S)

Dr. Olga Igoucheva, Ph.D.

5d. PROJECT NUMBER

5e. TASK NUMBER

5f. WORK UNIT NUMBER

7. PERFORMING ORGANIZATION NAME(S) AND ADDRESS(ES)

Thomas Jefferson University
Philadelphia, Pennsylvania 19107-5567

8. PERFORMING ORGANIZATION REPORT NUMBER

9. SPONSORING / MONITORING AGENCY NAME(S) AND ADDRESS(ES)

U.S. Army Medical Research and Materiel Command
Fort Detrick, Maryland 21702-5012

10. SPONSOR/MONITOR'S ACRONYM(S)

11. SPONSOR/MONITOR'S REPORT NUMBER(S)

12. DISTRIBUTION / AVAILABILITY STATEMENT

Approved for Public Release; Distribution Unlimited

13. SUPPLEMENTARY NOTES

14. ABSTRACT Development of chronic wounds is very common for patients affected by hereditary Epidermolysis Bullosa (EB). To date, there is still a substantial gap in understanding of the cellular events occurring during progression of wounds from early to poorly healing, and chronic wounds. To understand the dynamics of the inflammatory infiltrates at EB skin wounds and, possibly, delineate leukocytic cells, which are responsible for stalled wound repair, we conducted comprehensive FACS-based assessment of leukocytic populations associated with different stages of EB wound progression. Our analysis has determined that EB skin wound bed is associated with $CD11c^+$ antigen presenting cells (20%), $CD11b^+$ mature neutrophils (38%) and macrophages (7%), and T cells (40%). Remarkably, the majority of $CD11c^+$ antigen presenting cells (80%), including $CD207^+$ Langerhans cells, express CD80 activation marker and the majority of the $CD4^+$ and $CD8^+$ T cells are represented by $CD45RO^+$ effector T cells. In addition, our data demonstrated activation of adaptive immunity toward bacterial antigens in EB-associated wounds, immune-mediated targeting of infected host cells, and Treg-mediated inhibition of T cell responses toward bacterial antigens. Our findings suggest that adaptive immunity plays an important role in clearing bacterial infection in EB wounds.

15. SUBJECT TERMS
Epidermolysis Bullosa, wound healing, microbiome

16. SECURITY CLASSIFICATION OF:			17. LIMITATION OF ABSTRACT	18. NUMBER OF PAGES	19a. NAME OF RESPONSIBLE PERSON
a. REPORT	b. ABSTRACT	c. THIS PAGE			USAMRMC
U	U	U	UU		19b. TELEPHONE NUMBER *(include area code)*

Table of Contents

Page

1. INTRODUCTION

Epidermolysis bullosa (EB), a heterogeneous group of mechanobullous disorders, is characterized by fragility of the skin. Tissue separation manifesting as blistering of the skin and mucous membranes in different variants of EB takes place at the level of the cutaneous basement membrane zone (BMZ) at the dermal-epidermal junction (DEJ). Despite extensive studies of EB genetics and testing various therapeutic approaches to cure the disease, only palliative care revolving around judicious use of protective garments, bandages, and antibiotic creams is available to EB patients. Separation of skin layers following minor trauma to the skin is a hallmark of the disease. It leads to the development of blisters, erosions and non-healing wounds, which are associated with numerous complications including infection, sepsis, dehydration, deformities, and cancer. Although many EB skin blisters and erosions progress to skin wound, at present, there is no objective measure to predict whether a wound will heal or become chronic. Our previous findings indicate that blistering and wounded EB skin is characterized by an excessive production of several pro-inflammatory chemokines and deregulated recruitment of the leukocytes, particularly neutrophils, to the damaged skin. This is accompanied by the activation of adaptive and innate immunity triggered by wound colonizing bacteria and release of extracellular matrix (ECM) remodeling enzymes from the recruited neutrophils. In turn, secreted enzymes in blister fluids and wounds continuously degrade ECM and generate ECM-derived damage associated molecular patterns (DAMPs) that activate toll-like receptors (TLRs) on fibrocytes, and create a pro-inflammatory feedback loop. In case of a skin injury, when physical segregation between the host and microbiota is destroyed, the immune system could be overwhelmed by the volatile situation - when pathogens and commensals share the same inflamed environment and may negatively affect wound heling, particularly in EB-affected skin compromised by the abnormal DEJ. As adequate T cell responses are essential for immune-mediated protection against microbiota, we suggest that a high number of activated T cells at wound sites can either exhaust or establish tolerance toward wound-colonizing bacteria. Together, these events create a favorable milieu for the persistent inflammation, excessive digestion of the ECM, abrogation of keratinocyte motility, wound re-epithelization, and fibrosis. To date, no study has investigated these dynamics in EB blisters and wounds. Our current studies are designed to assess the complexity of the molecular and cellular interactions influencing the development of non-healing wounds on EB genetic background, and to delineate therapeutic intervention approaches. During first year of the project, we leveraged the ability of our clinical collaborator, Dr. J. Salas, to follow particular wounds on patients affected by different EB types while providing standard of care and our capacity to characterize healing capacities of EB-associated wounds on different genetic backgrounds. Also, to define microbial biomarkers predictive of the wound outcome, we initiated studies on the dynamics of bacterial and fungal communities during wound progression and healing. Ultimately, these studies will allow us to delineate molecular and cellular activities/mechanisms, which inhibit wound healing process.

2. KEYWORDS

EB - Epidermolysis Bullosa
EBS - Simplex Epidermolysis Bullosa
JEB - Junctional Epidermolysis Bullosa
DEB - Dystrophic Epidermolysis Bullosa
ECM - Extracellular Matrix
BMZ - Basement Membrane Zone
DAMPs - Damage Associated Molecular Patterns
ELR - Glu-Leu-Arg (ELR) Motif
TLRs - Toll-like Receptors
BF - Blister Fluids
FnEDA - Fibronectin Extra Domain A
APC - Antigen Presenting Cells
Ag - Antigens
CTL - Cytotoxic T Lymphocytes
PBMC - Peripheral Blood Mononuclear Cells
FACS - Fluorescence Activated Cell Sorting
ELISA - Enzyme-linked Immunosorbent Assay

HMW - High Molecular Weight
LMW - Low Molecular Weight

3. OVERAL PROJECT SUMMARY

Development of chronic wounds is very common for patients affected by hereditary Epidermolysis Bullosa (EB). To date, there is still a substantial gap in understanding of the cellular events occurring during progression of wounds from early to poorly healing, and chronic wounds. To understand the dynamics of the inflammatory infiltrates at EB skin wounds and, possibly, delineate leukocytic cells, which are responsible for stalled wound repair, we conducted comprehensive FACS-based assessment of leukocytic populations associated with different stages of EB wound progression. Our analysis has determined that EB skin wound bed is associated with $CD11c^+$ antigen presenting cells (20%), $CD11b^+$ mature neutrophils (38%) and macrophages (7%), and T cells (40%). Remarkably, the majority of $CD11c^+$ antigen presenting cells (80%), including $CD207^+$ Langerhans cells, express CD80 activation marker and the majority of the $CD4^+$ and $CD8^+$ T cells are represented by $CD45RO^+$ effector T cells. In addition, our data demonstrated activation of adaptive immunity toward bacterial antigens in EB-associated wounds, immune-mediated targeting of infected host cells, and Treg-mediated inhibition of T cell responses toward bacterial antigens. Our findings suggest that adaptive immunity plays an important role in clearing bacterial infection in EB wounds.

4. KEY RESEARCH ACCOMPLISHEMNTS

Specific Aim 1. To conduct longitudinal analysis of secretome in epidermolysis bullosa (EB) healing and non-healing wounds and define the role of leukocytic and fibrocytic infiltrates.
Major Task 1: Cross-sectional and longitudinal evaluation of secretome in healing and non-healing EB wounds.
Subtask 1: **S**ample collection and evaluation of wounds in EB-affected patients. Timeline - 18 months (1-18).
Per SOW: Wound-dressing bandages will be collected during routine re-dressing of the wounds at Dr. Salas's clinic. Demographic data, EB type, age of the wound will be documented by attending physicians at Dr. Salas's clinic. At least 40 patients with each type of wound (fresh, established or chronic) will be used for cross-sectional analysis during the observational period of about one year. At least 40-50 patients with each type of wound (fresh, established or chronic) will be used for longitudinal analysis with 8 to 12 repeated measures per wound during the observation period of about one year and a half. To rigorously investigate any potential sex bias, all experiments will be done in male and female cohorts.

Table 1. Sample collection of EB patient-derived material during first year of funding.

Analysis	Cross-sectional			Longitudinal		
Wound type	Early	Established	Chronic	Early	Established	Chronic
Assay type						
FACS: Wound-derived leukocytes	22	9	12	22	7	In progress
Multiplex ELISA: Wound-derived secretome	23	12	15	23	7	
High molecular weight fraction (HMW)	22	9	12	22	7	
Low molecular weight fraction (LMW)	23	12	15	23	7	
Wound-derived cells (total bandage-derived population)	10	5	8	10	N/A	
Wound-derived fibroblast-like cells	N/A	12	13	N/A	N/A	
Wound-derived T lymphocytes	3	4	5	3	N/A	
Wound-swabs for bacterial microbiome	33	22	48	33	17	
Wound-swabs for fungal microbiome	33	22	48	33	17	

Progress: The project started on September 1, 2018 (official award notice date). During the first twelve months of funding, we achieved the substantial progress in several aspects of the Specific Aims 1 and 2 of the project. As the most essential component of the project is samples (wound-covering bandages) from patients suffering with various forms of EB, first, we established very close interaction/collaboration with the clinician in EB area, Dr. Julio Salas (Mexico). Wound-dressing bandages and wound swabs were collected during routing re-dressing of the wounds. As a majority of EB patients uses regular gauze, all samples were normalized with regard to wound dressing material. Clinician also documented use of petroleum gel or Mupirocin cream (for chronic wounds). During each visit, the patients were asked to describe the natural history of each sampling site. Also, at each visit, wounds were coded and documented by description to include body site, antibiotic treatment (local or systemic), other drugs received and creams applied, as well as overall appearance of the wound.

Gauze (bandage) directly exposed to the wound bed was excised by attending physician, placed into a tube with transport media supplemented with Penicillin/Streptomycin/Amphotericin B and sent to the Dr. Igoucheva's laboratory. Immediately upon arrival to the laboratory, bandages were processed for the isolation of cellular and secreted components. Briefly, bandage-harbored cells were collected by scraping and centrifugation using aseptic techniques in the tissue culture hood. Resultant cell pellets were partially used for immediate FACS analysis and frozen cell stocks were made for future assays. Meanwhile, transport media was clarified by filtration on 0.22 microns filters, and subsequently concentrated on a 100 kDa cut-off centrifugal device to obtain a high molecular weight (HMW) fraction and a 10 kDa Amicon filter fraction (low molecular weight (LMW) fraction). Concentrated LMW fractions were stored at -80^0 C for the assessment of the secretome by Multiplex ELISA assay, whereas HMW fractions were stored at -80^0 C for the analysis of larger molecules (e.g. fibronectin extra domain A, FnEDA) by Western blot analysis. Our established protocol permitted the retrieval on average $1x10^6$ - $6x10^6$ cells from a single bandage with an equal distribution (50/50) of leukocytic and fibroblastoid infiltrates. The status of patient-derived samples is presented in the Table 1. As of note, the Table 1 reflects only the samples collected up to date. Since longitudinal studies are still underway, more samples are expected in next 6 months.

Subtask 2: Analysis of secretome activity in early, established and chronic wounds. Timeline - 18 months (1-18).
Per SOW: Bandage transport media from wound dressings will be collected, clarified and concentrated for secretome analysis. Composition of EB secretomes will be evaluated by Multiplex ELISA assays. Secretome activity of various EB wounds on recruitment of various inflammatory cells will be evaluated using various FACS-based protocols.

Progress: Cytokine networks can be interrogated effectively using LEGENDplex bead-based immunoassays. These assays are based on the same principle as the sandwich Enzyme-Linked Immunosorbent Assay (ELISA), and use fluorescence encoded microspheres with capture antibodies covalently attached to their surface. These antibodies are immobilized on surface areas much smaller than those required by traditional ELISA formats. Briefly, capture beads, which can be differentiated by size and internal allophycocyanin fluorescence intensity, are conjugated to antibodies specific to a particular analyte. Next, a selected panel of defined capture bead sets is incubated with a biological sample containing target analytes specific to the capture antibodies. A biotinylated detection antibody cocktail is added, which leads to the formation of capture bead-analyte-detection antibody sandwiches. Finally, streptavidin-phycoerythrin is added, which binds to biotinylated detection antibodies, providing fluorescent signal intensities in proportion to the amount of bound analyte. The PE fluorescent signal of analyte-specific beads regions is quantified using flow cytometry, and the concentrations of particular analytes are determined using data analysis software and the standard curve generated in the assay. This enables such assays to be performed with far less sample volume, while at the same time reducing non-specific binding and providing multiplexed analysis of several analytes. BioLegend's LEGENDplex™ kits are provided as predefined panels. Each kit provides sufficient reagents for at least 100 tests. The assay is performed in FACS tubes, allowing running 40 samples plus 8 standard curve titrations in duplicate (96-sample format). In our upcoming experiments, we plan to use several panels (Human Inflammation panel (13-plex), Human Growth factor panel (13-plex), Human proinflammatory chemokines (13-plex), HU Th cytokine panel (13-lex), and HU Th17 panel (8-lex)) to simultaneously quantify the cytokine targets in LMW fractions collected from bandage-derived transport media (Table 1). All LEGENDplex™ kits are already purchased. Currently, we are waiting for remaining samples from

longitudinal studies. Once we have all samples in place, multiplex ELISAs will be run simultaneously to provide results that are accurate and statistically significant.

Major Task 2: Cross-sectional and longitudinal analyses of cellular infiltrates in EB healing and non-healing wounds.

Subtask 1: Characterization of cellular infiltrates at the sites of healing and non-healing EB skin wounds. Timeline - 18 months (1-18).

Per SOW: Wound-associated bandage-derived cells will be isolated concurrently with the secretome using cell-specific techniques. Evaluation of wound-associated cell populations will be done using FACS-based protocols.

Progress: EB skin wounds contain all major leukocytic populations, including activated $CD4^+$ and $CD8^+$ T cells. To get a better insight of the inflammatory infiltrates associated with EB wounds, first, we evaluated wound bed-associated

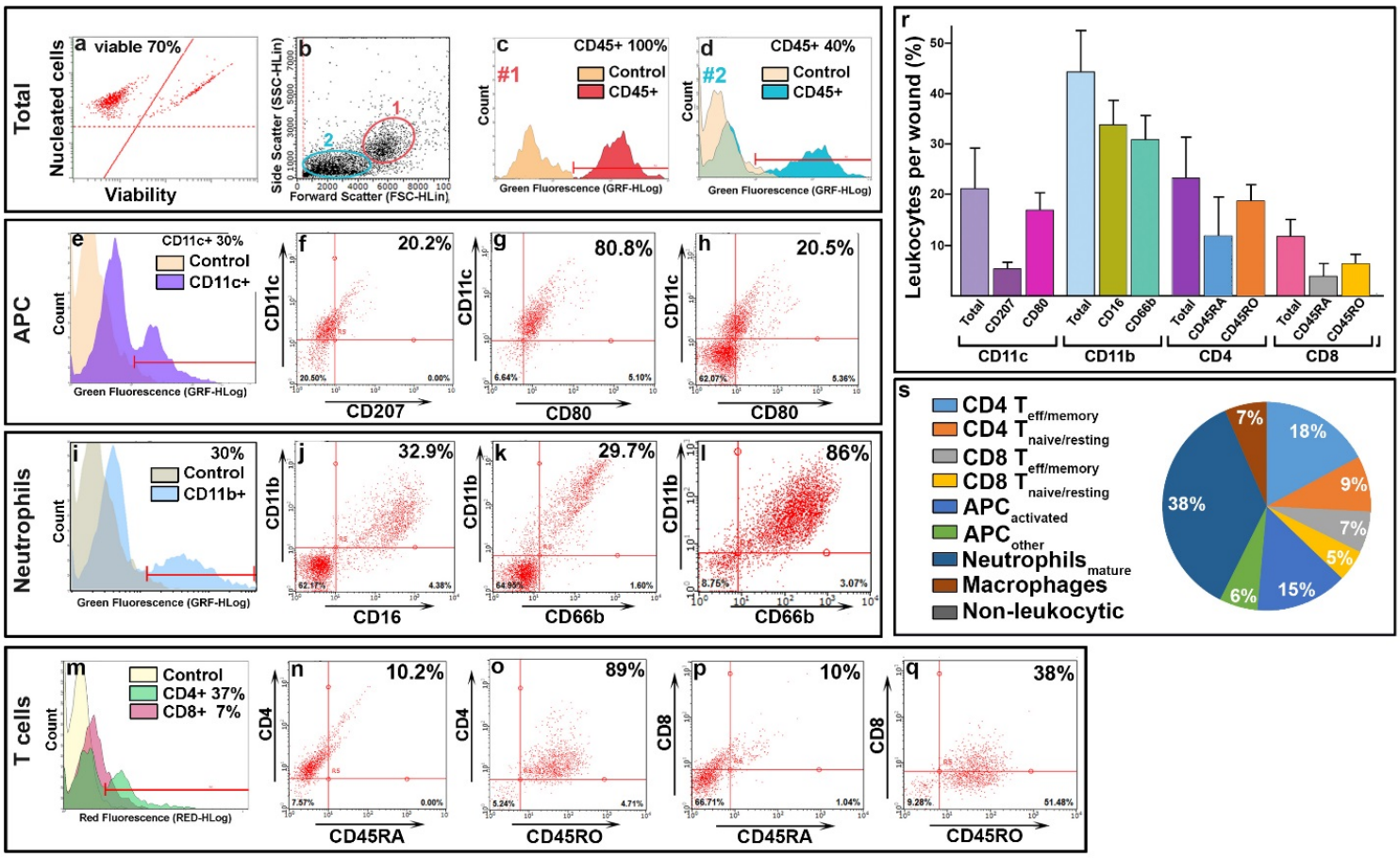

Figure 1. Analysis of bandage-derived leukocytes. (a) Density plot illustrating viability of bandage-recovered cells. Percentage of viable cells is shown on the plot. (b) Light scatter density plot depicting two distinct populations in bandage-derived cells. Populations are outlined and numbered. (c, d) Representative FACS profiles illustrating $CD45^+$ sub-populations in two populations of bandage-derived cells. Gated populations (#1 and #2) are color-coded as in (b). Percentage of $CD45^+$ cell is shown on histograms. (e-h) Analysis of bandage-derived $CD11c^+$ antigen presenting cells (APC) illustrating: (e) percentage of $CD11c^+$ APC in bandage-derived cells, percentage of $CD207^+$ Langerhans cells (f) and $CD80^+$ activated T cells (g) in $CD11c^+$ population and (h) percentage of $CD80^+$ APC in bandage-recovered cells. (i-l) Analysis of bandage-derived $CD11b^+$ myeloid cells showing percentage of $CD11b^+$ (**i**), $CD11b^+$ $CD16^+$ (j) and $CD66b^+$ (k) cells in a total population of bandage derived cells and percentage of the $CD66^+$ cells in $CD11b^+$ population (l). (m-q) Analysis of bandage-derived T lymphocytes showing percentage of $CD4^+$ and $CD8^+$ T cells in a total population of cells (m) and the presence of $CD45RA^+$ (naïve/memory) and $CD45RO^+$ (activated/effector) $CD4^+$ (q, r) and $CD8^+$ (s, t) T cells. On profiles and plots, detected antigens are show on X and Y-axes; percentages of double-positive cells are shown in the upper right quadrants. Histogram markers are placed to define a threshold of antigen-positive cells and detected antigens are shown in inserts. (r) Column chart showing percentages of specific leukocytes and sub-populations in cell recovered from bandages. Data is presented as average percentage ±SD. (s) Pie charts showing average distribution of specific leukocytic sub-population in bandage-derived leukocytes and in a total population of bandage-derived cells, as indicated. Percentages are shown in charts. Data is collected from cells recovered from 10 independent bandages.

leukocytes from wound-covering bandages disregarding wound status. Based on FACS viability data, most of bandage-recovered cells (on average 70%) were found to be viable (Fig. 1a). The light scatter versus forward scatter (SS vs FS) defined 2 distinct populations of varying size and complexity (Fig. 1b). The most prominent population of a higher complexity (about 50% of total recovered cells) was entirely (100%) comprised of $CD45^+$ cells (Fig. 1b, c; population #1). The population of a lower complexity (population #2) contained on average 40% of $CD45^+$ cells (Fig. 1c), presumably, T lymphocytes. These populations were consistently detected in at least 10 independent isolations. Immuno-phenotyping of bandage-derived cells revealed that about 30% of total recovered cells are $CD11c^+$ Antigen Presenting Cells (APC) (Fig. 1e), 10% to 20% of which were represented by CD207 (Langerin) Langerhans cells (Fig. 1f). Remarkably, over 80% of $CD11c^+$ cells also expressed CD80 APC activation marker and $CD11c^+CD80^+$ activated APC represented on average 17% of total cells recovered from bandages (Fig. 1g, h, r). Further assessment demonstrated that on average 44% of bandage-derived cells expressed $CD11b^+$ myeloid cell marker (Fig. 1i, r) and that the $CD11b^+$ population almost uniformly expressed CD16 and CD66b markers of the mature neutrophils (Fig. 1j, k). In fact, about 80-90% of $CD11b^+$ cells were identified as $CD11b^+CD66b^+$ mature neutrophils (Fig.1i). Immuno-phenotyping also showed that bandage-derived cells contain up to 30% of $CD4^+$ and up to 15% of $CD8^+$ T cells (Fig 1m, r). Both $CD4^+$ and $CD8^+$ bandage-derived populations contained about 10% $CD45RA^+$ memory/naïve T cells. $CD45RO^+$ activated/effector sub-population represented about 90% of $CD4^+$ and about 40% of $CD8^+$ T cells (Fig. 1n-r). Collectively, this analysis revealed that viable leukocytes could be successfully recovered from wound-covering bandages for the assessment of the wound bed-associated inflammatory cellular constituents. Collectively, FACS-based assessment determined that EB skin wound bed-associated leukocytes comprise of $CD11c^+$ APC (20%), $CD11b^+$ mature neutrophils (38%) and macrophages (7%), and T cells (40%). Remarkably, the majority of $CD11c^+$ APC (80%), including $CD207^+$ Langerhans cells, express CD80 activation marker and that the majority of the $CD4^+$ and $CD8^+$ T cells were represented by $CD45RO^+$ effector T cells (Fig. 1s).

To date, there is still a substantial gap in understanding of the cellular events occurring during progression of wounds from early to poorly healing and chronic wounds. To understand the dynamics of the inflammatory infiltrates at EB skin

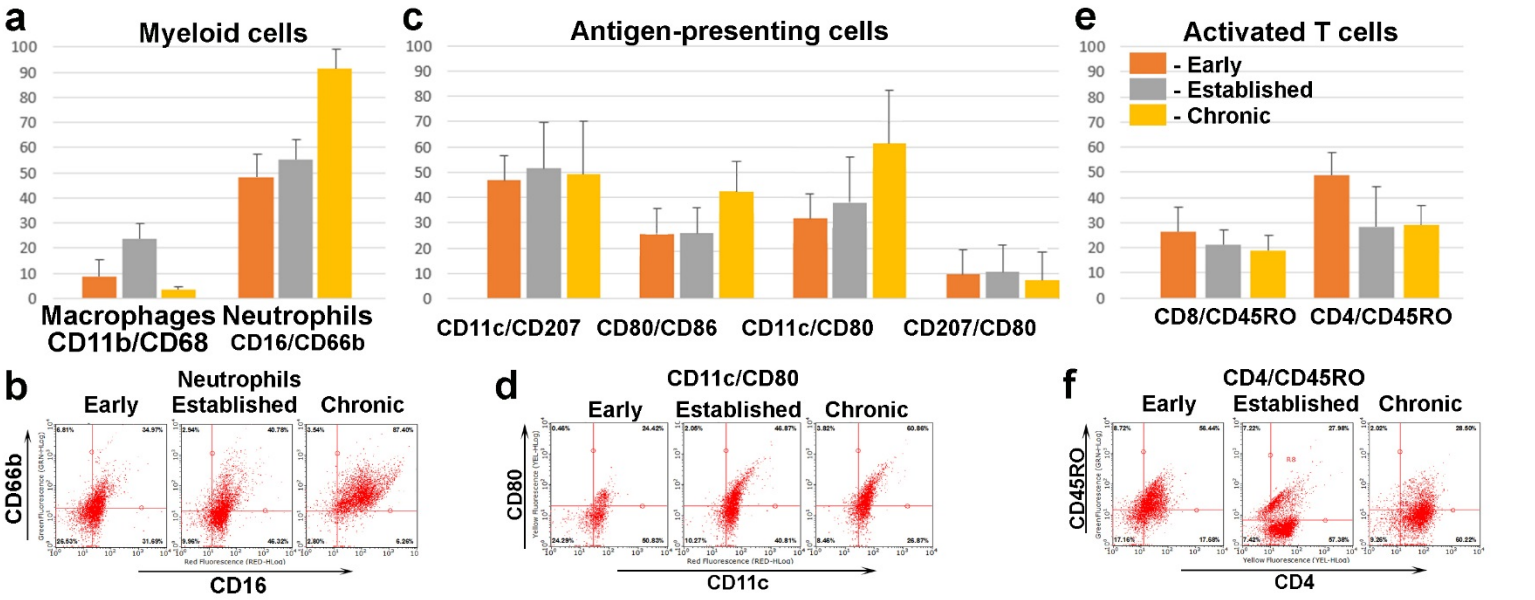

Figure 2. FACS-based analysis of EB wound-associated leukocytes. (a) Analysis of wound-associated myeloid cells including $CD11b^+CD68^+$ macrophages and $CD16^+CD66b^+$ neutrophils (as indicated below columns). (b) representative dot plots illustrating distribution of $CD16^+CD66b^+$ mature neutrophils in early, established and chronic wounds (as indicated) and accumulation of mature neutrophils in chronic wounds. (c) Analysis of wound-associated APC ($CD11c^+$ DC and $CD207^+$ LC) and their activation status as determined by detection of CD80 and CD86 markers on cell surface. (d) Representative dot plots depicting accumulation of activated $CD80^+$ APC in chronic wounds. (e) Analysis of wound-associated $CD8^+$ and $CD4^+$ T cells and their activation status. (f) Representative dot plots showing education of $CD45RO^+$ activated T cells in chronic EB wounds. In all column charts, the data is presented as an average percentage of cells associated with specific wound type ±SD, as determined by FACS-based quantitation. Detected antigens are shown below the columns. Wound types are color-coded, as shown in the key. In all representative dot plots, detected antigens (cell type-specific markers) are shown at X- and Y-axes. Percentages of cells positive for both markers are shown in the upper right quadrant.

wounds and, possibly, delineate which leukocytic cells are responsible for stalled wound healing, we further analyzed specific leukocytic populations associated with different stages of wound progression. Myeloid cells, specifically, neutrophils are the primary line of cellular defense at a time of skin injury. In physiological wound healing, these cells are rapidly recruited to the sites of injury within minutes, and cleared from the wounds through apoptosis within several days. When assessing accumulation of myeloid cells, we observed a rather low number of macrophages at EB wound sites as defined by FACS using CD11b/CD68 antibodies. We observed a substantial increase of these cells during establishment of EB skin wounds and an almost complete lack of macrophages in chronic wounds (Fig 2a).
At the same time, more than 50% of myeloid cells in early EB lesions were represented by $CD16^+CD66b^+$ neutrophils. Further progressive accumulation of mature neutrophils was observed in established and chronic wounds (Fig. 2b). Moreover, as illustrated by representative dot plots, percentages of $CD16^+CD66b^+$ cells are similar in early and established lesions but significantly increased in chronic wound (Fig. 2b). These findings confirmed our original hypothesis that accumulation of neutrophils in chronic wounds may negatively affect healing of EB wounds. The obtained data allowed us to launch a biostatistical modeling to estimate the value of neutrophils as a predictor of wound progression. FACS-based evaluation of $CD11c^+$ population of professional antigen presenting cells (APC) showed that it is equally represented by epidermal Langerhans cells (LC; $CD207^+$) and dermal dendritic cells (DC) in all types of wounds (Fig. 2c). Analysis of APC activation status showed that in early and established wounds 25% to 35% of APC express CD80 and CD86 activation markers with about 1/3 of activated APC represented by $CD80^+CD207^+$ LC. However, a substantial increase in activated APC, $CD11c^+CD80^+$ and $CD80^+CD86^+$, was detected in chronic wounds. As shown in representative dot plots (Fig. 2c), activation of $CD11c^+$ APC occurs during transition of early to established wounds (increase from on average 20% to 40% of $CD11c^+CD80^+$ cells, upper right quadrant) and during transition of established to chronic wounds (increase from on average 40% to 60% of $CD11c^+CD80^+$ cells, upper right quadrant). These findings suggest that during wound progression APC continue to acquire antigens. Considering that chronic EB wounds are frequently infected with different bacteria and fungi, we suggested that accumulation of microbial antigens in chronic wounds might trigger activation of adaptive immunity. FACS-based analysis of T cells in early, established and chronic wounds demonstrated a substantial presence of $CD45RO^+$ activated CD8 and CD4 T cells in early lesions. However, number of these cells decreased during progression to established wounds (Fig 2e), which was clearly detected as a separation of $CD45RO^+$ and $CD45RO^-$ populations (Fig. 2f). These findings indicate that there is an activation of T cells in early wounds, and, possibly, generation of peripheral immunologic memory. A more detailed immuno-phenotyping of effector and memory T cells in different wounds is still on-going. Taken together, analysis of leukocytic infiltrate in early, established, and chronic wounds confirmed our hypothesis regarding accumulation of neutrophils at wound sites and provided the foundation for the studies outlined in Specific Aim 2 of the project and relevant to the understanding of the microbial immune system interaction in the wounds. In fact, having on hand the obtained data and EB patient derived T cells, we already initiated a number of studies aimed at defining the role of adaptive immunity in controlling infection (see below, Major Tack 4).

Milestone(s) Achieved: A well characterized analysis of cellular infiltrates of EB-associated wounds.
Acquisition of statistically significant data. Achievement is expected in September 2020.

Specific Aim 2. To characterize microbial dynamics and immunogenicity of the wound colonizing bacteria.

Major Task 3: Analysis of bacterial microbiome in new, established and chronic wounds.
Subtask 1: Sample collection. Timeline - 12 months (1-16).
Per SOW: Wound swabs will be collected concurrently with wound-dressing bandages during routine re-dressing of the wounds at Dr. Salas's clinic using the Levine non-invasive technique. Demographic data, EB type, age of the wound/blisters will be documented by attending physicians at Dr. Salas's clinic. At least 40-50 patients with each type of wound (fresh, established or chronic) will be used for bacterial microbiome studies.

Major Task 4: Analysis of fungal mycobiome in new, established and chronic wounds.
Subtask 1: Sample collection. Timeline - 12 months (1-12).
Per SOW: Samples collected for microbiome studies will also be used for fugal assessment. At least 40-50 patients with each type of wound (fresh, established or chronic) will be used for fungal studies.

Progress: During progress period, we achieved both Subtasks 1 and 2 of Specific Aim 2. Microbiome samples were collected using the Levine technique concurrently with wound-dressing bandages as described above (Major Task 1, Subtask 1). EB-associated wounds were coded and documented to include body site, antibiotic treatment (local or systemic), other drugs received and creams applied, as well as overall appearance of the wound. Briefly, after cleansing wounds with non-bacteriostatic saline, a Floqswab (Copan) was rotated over a 1 cm^2 area of viable wound tissue in the center of the wound bed for five seconds to extract wound-tissue fluid. Upon collection, all swabs were stored in liquid nitrogen (~ -196^0 C) until analysis. Samples collected over time are presented in Table 1. Currently, we are setting up service with the CHOP Microbiome Center (Philadelphia, PA) for further DNA isolation, sequencing and bacteriome and mycobiome analyses as described in the project.

Major Task 4: Analysis of microbiota immunogenicity and adaptive cell immunity at wound site.
Subtask 1: Assessment of microbiota-specific T cells in early, established and chronic wounds. Timeline - 12 months (13-18).
Per SOW: Functional profile of bacteria-specific T cells will be evaluated by Multiplex ELISA assays.

Subtask 2: Analysis of the microbiota-induced immunosuppression. Timeline – 12 months (18-24).
Per SOW: Differentiation and activation of the bandage-derived T cells at different stages of wound progression will be assessed by FACS. Cytokine production and secretion by activated T cells will be analyzed by ELISA and ELISpot assays.

Progress: During progress period, we already initiated studies outlined in Specific Aim 2, Major tack 4, Subtasks 1 and 2. EB patient-derived microbial antigens (Ag) stimulate T cell proliferation. To assess the presence of microbial antigen-responding T cells in EB wounds, T cells were isolated from bandages and propagated *in vitro*. Initial FACS-based

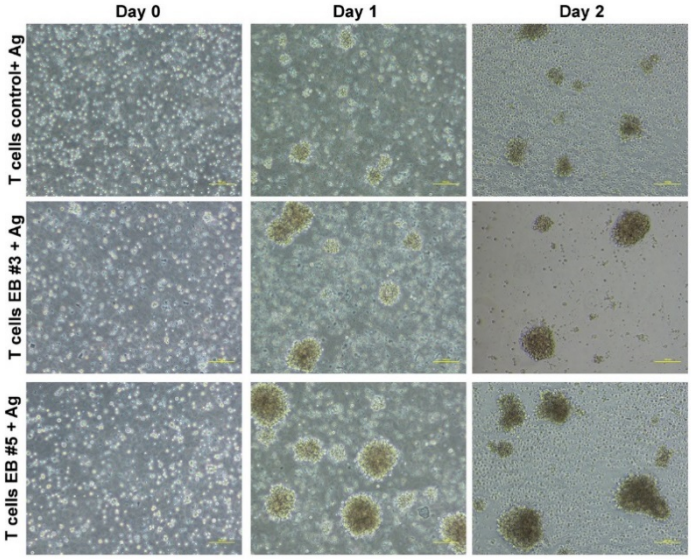

Figure 3. Microscopic analysis of the T cell proliferation after exposure to microbial antigens. Microscopic analysis of the T cell proliferation after exposure to microbial antigens. Duration of exposure to microbial antigens is shown above the panels. Control and EB-derived T cells exposed to Ag are indicated to the left. T cells clones are visualized as large suspended colonies. Scale bar – 10 µm.

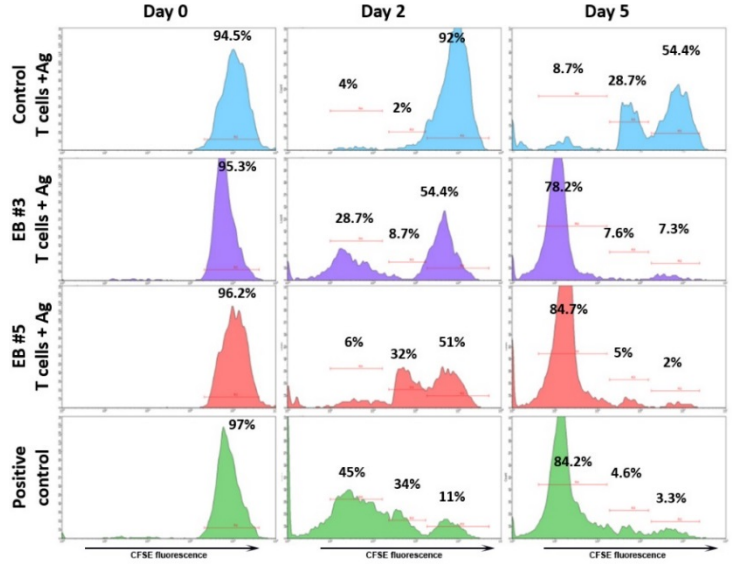

Figure 4. CFSE dilution assay for the quantitation of T cell proliferation after exposure to microbial antigens.

SCFSE dilution assay. All panels show representative profiles of the FACS-based analysis of T cell division using CFSE dilution assay. Profiles illustrate changes in fluorescence intensity in proliferating T cell population, as reflected by the shifts of the fluorescent pikes to the left. Days of exposure are show on top of the panels. Control and RDEB-derived cells are shown to the left of the panels. Percentages of T cell populations relative to a total number of cells are shown above

assessment demonstrated that $CD4^+$ and $CD8^+$ T cells represented on average 90% and 10% of total T cell population, respectively. Exposure of cells to microbial antigens resulted in the induction of T cell proliferation. All EB-derived T

cells responded to microbial Ag within the first 24 hours. Exposure for additional 24 hours resulted in the formation of T cell colonies, suggesting clonal expansion of the microbial Ag-specific T cells. Although some colony formation was detected in control T cells exposed to bacterial Ag, EB patient-derived T cell colonies were substantially larger than controls (Fig. 3). To better assess induction of T cell proliferation, a standard CFSE dilution assay was utilized. This assay confirmed microscopic observations. Exposure of T cells to microbial Ag stimulated proliferation of EB T cells but did not substantially affect control T cells (Fig. 4). FACS based quantitation showed that two days of Ag exposure induced proliferation in, on average, 3% of control and 35% of RDEB T cells (Fig. 4). Within this time, about 80% of positive control cells exposed to IL-2 and anti-CD3/CD28 stimulants were proliferating. An additional three days of exposure led to a substantial proliferation of EB cells (~80% average) and only partial (~35% average) proliferation of control cells (Fig. 4). Collectively, this set of studies demonstrated microbial antigen-dependent induction of T cell proliferation.

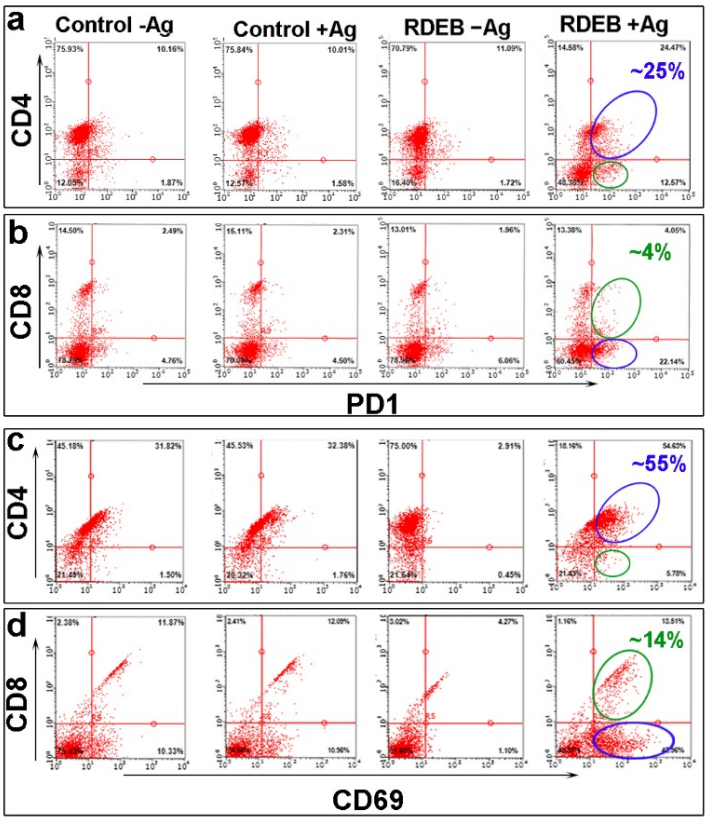

Figure 5. FACS-based analysis of activation-specific cell surface markers (PD-1 and CD69) on T cells exposed to microbial Ag. Induction of PD-1 (a, b) and CD61 (c, d) expression on $CD4^+$ and $CD8^+$ T cells (as indicated to the left of the panels) was detected by FACS analysis. Representative density plots with quadrant markers are shown on panels. Percentages of CD4 and CD8 T cells positive for PD-1 and CD69 (upper right quadrant) are shown on panels. Treatments and controls are indicated above the columns of panels.

Microbial antigens reactivate a pool of EB patient-derived T cells. Activation of T cells is a multistep process characterized by changes in the expression of various cell surface makers. To investigate whether T cells are activated by microbial Ag, induction of CD69 and PD1 on the surface of microbial Ag-exposed patient-derived and control T cells was examined. Exposure of control T cells to microbial Ag did not induce PD1 expression. However, incubation of the EB-derived T cells with microbial Ag led to the induction of PD1 in 15-25% of $CD4^+$ T cells. This induction was observed as early as two days of exposure (Fig. 5). Some insignificant induction of PD1 on the surface (about 4%) of $CD8^+$ EB patient-derived T cells was also observed (Fig. 3b). When assessing CD69, an early marker of T cells activation, a substantial induction was observed in $CD4^+$ EB T cells (about 50%) and in $CD8^+$ EB T cells (about 13%). Although background cell surface CD69 was detected in control $CD4^+$ T cells (on average 30%) and in $CD8^+$ T cells (on average 10%), addition of microbial Ag did not alter cell surface expression of this marker. These analyses also demonstrated that EB-derived T cells contain a pool of cells, which are activated by microbial Ag.

Microbial antigens induce IFNγ production by T cells and T cell degranulation. It is well established that T cell activation leads to a production of pro-inflammatory cytokines such as IL-2 and IFNγ. It can also result in degranulation (release of the cytotoxic

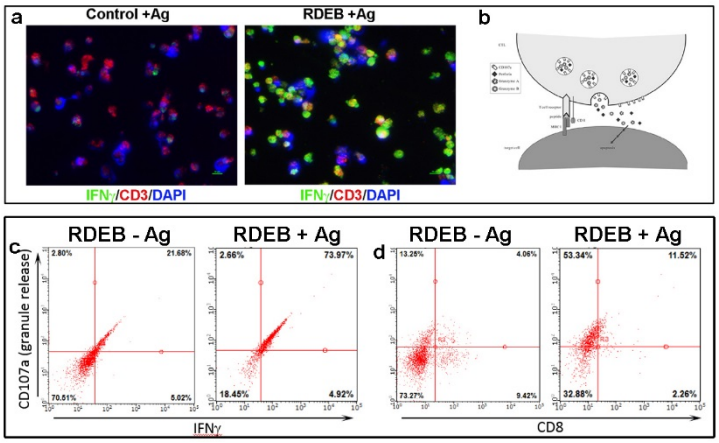

Figure 6. Analysis of IFNγ production and T cell immune-fluorescence staining and FACS analyses using IFNγ and CD107a-specific antibodies. Indirect immunofluorescence and FACS analyses of T cells exposed to microbial antigens. (a) Indirect immunofluorescence detection of IFNγ in control and DEB-derived T cells exposed to microbial antigens. Detected antigens are shown below representative micrographs in corresponding colors. Scale bar – 100 μm. (b) Diagram depicting exposure of the CD107a on the surface of T cells during degranulation. (c) FACS-based analysis of CD107a and IFNγ in DEB T cells exposed to microbial antigens (as indicated above the panels). Representative density plots depict CD107a and IFNγ expression in a total T cell population (2 panels to the left), and induction of CD107a in CD8 T cells (2 panels to the right). Percentages are shown on panels.

granules) particularly by $CD8^+$ cytotoxic T cells. To assess whether expression of proinflammatory cytokines is induced in EB-derived T cells by microbial Ag and evaluate degranulation of the T cells, intracellular cytokine staining assay was employed. Along with detection of the intracellular cytokines by fluorescently labeled antibodies, CD107a was also detected as a marker of granule release. This protein is present in the inner surface of the granules and is hidden from detection by antibodies. Yet, when T cells are activated, granules are fused with plasma membrane to release granules and the inner surface of the granules with CD107a become accessible to the antibodies (Fig. 6b).
Initially, T cells were exposed to the microbial Ag overnight in the presence of Golgi plug (for accumulation of the cytokine in the cells). Indirect immunofluorescent detection was used to detect intracellular IFNγ. This assessment

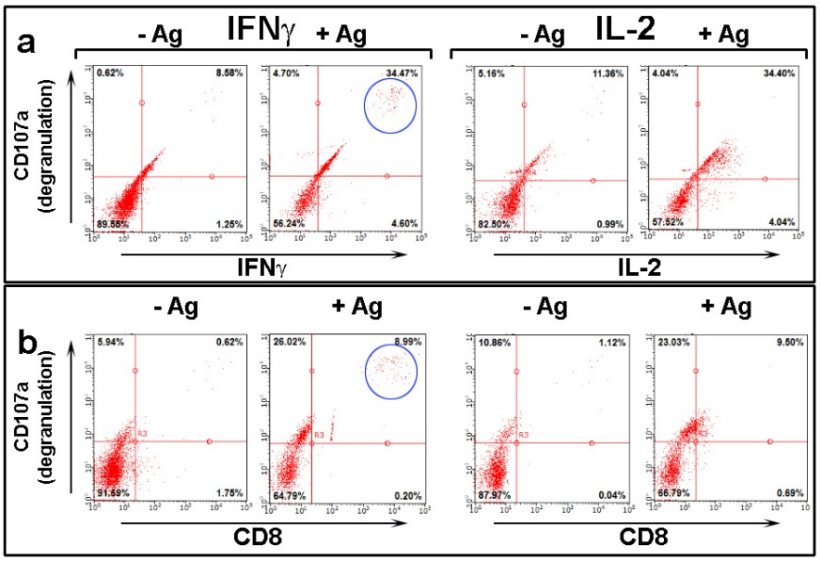

Figure 7. Intracellular staining of the IFNγ and IL-2 in T cells exposed to microbial antigens detected by FACS. Assessment of the proinflammatory cytokines in antigen-exposed RDEB T cell. (a) Induction of IFNγ and IL-2 detected by the ICS along with the induction of degranulation detected by CD107a-specific antibodies. (b) Induction of degranulation of CD8+ T cells after exposure to microbial antigens. On all panels, conditions (+ / - antigen) are shown above panels; detected antigens are shown on Y and X axes; a population of CD8+CD107a+ cells in Ag- exposed T cells is outlined. Representative density plots depict distribution of T cells.

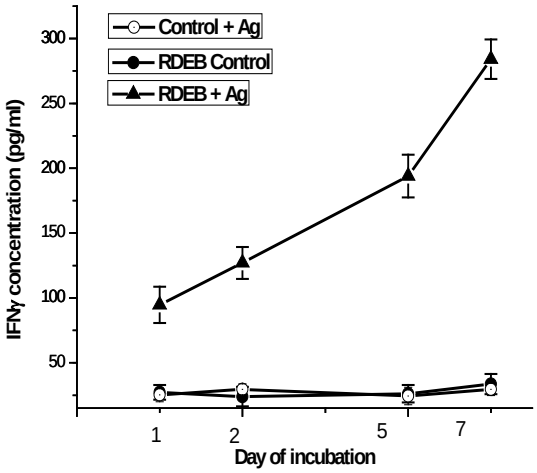

Figure 8. ELISA-based analysis in IFNγ secretion from T cells exposed to microbial antigens. Quantitation of IFNγ secretion by Ag-exposed RDEB T cells. Graph illustrate changes in IFNγ secretion from microbial antigen-exposed RDEB and control T cells (as indicted on the key). Data is presented as an average of 2 independent experiments run in triplicates +/- SD.

showed a substantial induction of the cytokine after overnight exposure of T cells to the antigens (Fig.6a). Then, IFNγ intracellular staining was employed. FACS-based assessment showed that about 20% of control cells were $CD107a^+$ $IFN\gamma^+$ after overnight exposure to microbial Ag. At the same time, about 70% of EB-derived T cells were positive for both markers. When assessing IFNγ in $CD8^+$ T cells, about 10% of $CD107a^+$ and $IFN\gamma^+$ T cells were detected (Fig.6c,d). This data confirms antigen-specific activation of a small population of $CD8^+$ cytotoxic T cells. Additional intracellular staining of the EB-derived T cells showed that their exposure to microbial Ag induces expression of both IFNγ and IL-2 (Fig.7a). Of particular interest, is the detection of a small population of $CD8^+$ T cells, which were highly positive for CD107a and IFNγ (Fig.7a,b). This analysis also showed that there is an induction of IL-2 expression in patient-derived T cells after exposure to microbial Ag (Fig. 7a,b). To validate production of pro-inflammatory cytokines by EB-derived T cells after exposure of cells to the microbial Ag, the secretion of IFNγ and IL-2 was evaluated using cytokine-specific ELISA assays. As shown in Figure 8, IFNγ in rapidly induced in EB-derived T cells upon exposure to microbial Ag, whereas no substantial induction was observed in cultured EB T cells without Ag stimulation. No substantial IFNγ induction was detected in control T cells exposed to microbial Ag (Fig. 8). This data additionally confirmed T cell activation by microbial antigens. However, despite observed induction of IL-2 expression, as detected by the intracellular staining, no substantial increase in secreted IL-2 was detected in the media collected from microbial Ag-exposed cells. This observation could be explained by the absence of

the additional T cell stimulation in the *in vitro* conditions, which in physiological conditions is provided by professional antigen presenting cells.

Staphylococcus Aureus antigens is recognized by T cell-mediated immunity in RDEB skin. To better define which microbial Ag could be targeted by the adaptive immunity and activate T lymphocytes, the presence of most common microbial contaminants in bandage-derived cells was evaluated using polymerase chain reaction (PCR). Using a set of

Table 2. PCR-based analysis of microbial contamination of RDEB wounds[#].

Wound type/age	*Pseudomonas Auruginosa*	*Entero Feacialis*	*Streptococcus group A*	*Proteus Mirabilis*	*Staphylococcus Aureus*	*Staphylococcus Epidermis*	*Escherichia coli*	*Candida Albican*	*Candida Parapsilosis*	*Mycoplasm*
chronic	***				***					**
early					*					
chronic					*					
chronic										
early										
chronic										
established										
established					**					
early					*					
established					*					
chronic					**	***				
early					*					
chronic					**					
early					****	**				
chronic					***					
early										
1 day						**				
chronic					***					
early										
early						**				

Range of detection: * - hardly detectible; **** - highly positive

PCR primers specific to several bacterial and fungal species, multiple bandage-derived cells were examined for the

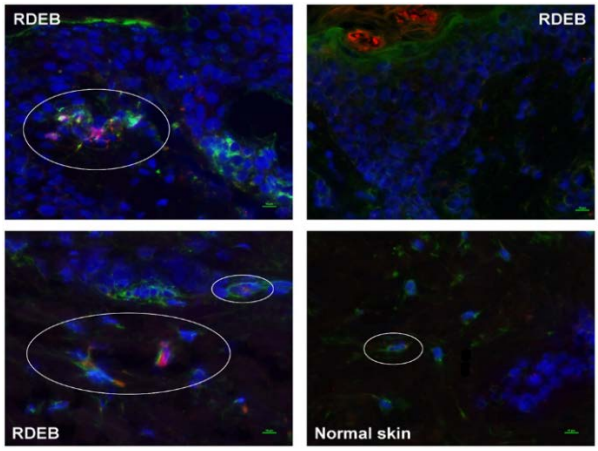

Figure 9. Detection of *Staphylococcus Aureus* in normal and DEB-affected skin. Indirect immunofluorescence analysis of *Staphylococcus Aureus* in normal and DEB-affected skin. S.aureus was detected inside DEB skin and on the surface (red) often in association with CD11b+ cells (green) (macrophages). Some *Staphylococcus Aureus* specific signals were detected in normal human skin. DEB and Normal skin samples are indicated on panels. *Staphylococcus Aureus* - positive area in the skin if encircled. Scale bar – 50 µm.

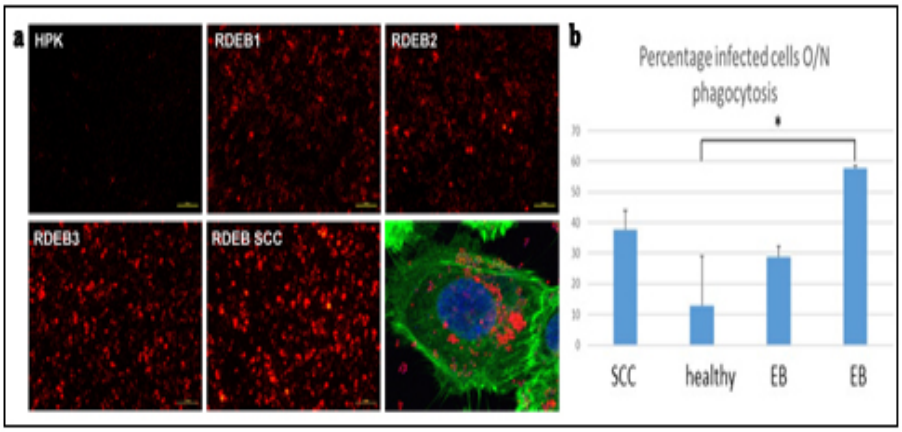

Figure 10. Analysis of keratinocyte infectivity by *Staphylococcus Aureus in vitro*. (a) Direct detection of fluorescently labeled *Staphylococcus Aureus* after overnight incubation with normal human primary keratinocytes (HPK), recessive dystrophic EB (RDEB) keratinocytes from the skin of RDEB patients, and from RDEB-derived squamous cell carcinoma (RDEB SCC). Intracellular bacteria is visualized as an aggregation of red fluorescent signals. Scale bar - 100 µm. Confocal imaging confirming intracellular location of the *Staphylococcus Aureus* (Red) in RDEB SCC-derived keratinocytes. Blue - DAPI nuclear staining; Green - actin filament staining with phalloidin. (b) Quantitation of infectivity of human primary keratinocytes (healthy), recessive dystrophic EB keratinocytes (from two patients), and SSC RDEB. Images of three different fields per cell culture were taken and quantified using Photoshop software.

presence of these microbes. This analysis demonstrated the presence of several bacterial species in wound site-derived cells with *Staphylococcus Aureus* being the most prominent (Table 2).

This preliminary data suggest that *Staphylococcus Aureus*-derived Ag could be the primary target for the adaptive immunity, particularly cytotoxic T lymphocytes (CTL). This suggestion is strongly supported by prior studies showing that *Staphylococcus Aureus* contains some super Ag recognizable by adaptive immunity, and that these species can infect keratinocytes and escape from autophagosomes into the cytoplasm. Based on these published data and our observations, we suggest that microbial Ag-induced T cells, particularly CTL, can target *Staphylococcus Aureus*-infected cells in EB skin. To evaluate this hypothesis, the presence of *Staphylococcus Aureus* in normal and DEB affected skin was examined by indirect immunofluorescence. This assessment demonstrated that *Staphylococcus Aureus* could be detected in normal and DEB skin in co-localization with CD11b+ myeloid cells (presumably, macrophages) (Fig. 9). Although *Staphylococcus Aureus*-positive staining was detected in normal skin, this bacteria was more frequently detected in DEB skin. Considering that cells like macrophages and neutrophils are well-equipped to destroy phagocytosed bacteria, it was suggested that other cells, like keratinocytes, could be infected by bacteria at wound sites and could be targeted by bacteria-specific CTL. To validate whether bacteria can infect DEB-derived keratinocytes, an *in vitro* infectivity assay was employed. When inactivated, fluorescently-labeled *Staphylococcus Aureus* was incubated with normal and DEB keratinocytes overnight. A substantial difference was detected in the intracellular bacteria-derived fluorescent signals. Substantially higher fluorescence was observed in RDEB cells, particularly those, derived from DEB squamous cell carcinoma (RDEB SSC) (Fig. 10a, b). Intracellular location of the infected cells was verified by confocal fluorescence microscopy (Fig. 10a). These findings suggest that *Staphylococcus aureus*-specific T cells could target infected keratinocytes at wound sites. However, at this time point, further validation of this suggestion will require more patient-derived material. This work continues.

5. OPPORTUNITIES FOR TRAINING AND PROFESSIONAL DEVELOPMENT
Nothing to report

6. IMPACT
It is anticipated that the proposed cross-sectional and longitudinal analyses will allow us to define precipitating factors, which predefine abnormal wound healing in EB skin lesions. In the short term, these investigations will allow us to develop clinically relevant tests and algorithms to assess wound healing capacities of the EB-associated wounds. Analysis of the microbiome and concurrent cellular infiltrates will also permit better selection of antibiotic and antiseptic creams/ointments to restore microbiota balance and decrease inflammatory response. In the long term, the obtained data will pave the path to the development of novel therapeutic approaches aimed at prevention and management of chronic wounds focused on reduction of inflammation and fibrosis.

7. CHANGES/PROBLEMS
Nothing to report

8. PRODUCTS
We have two manuscripts in preparation (provided titles are tentative):

Huitema, L., Phillips, T., Salas-Alanis, J.C., Chervoneva, I., Uitto, J., Alexeev, V., Igoucheva, O. “Disease-site activities impairing wound healing in hereditary epidermolysis bullosa”.

Huitema, L., Phillips, T., Salas-Alanis, J.C., Debes, G., Chervoneva, I., Uitto, J., Alexeev, V., Igoucheva, O. “T cell-mediated immunity in hereditary epidermolysis bullosa”.

9. PARTICIPANTS AND OTHER COLLABORATIG ORGANIZATIONS

Name:	Olga Igoucheva	Vitali Alexeev	Leonie Huitema	Jouni Uitto	Gudrun Debes	Taylor Phillips

Project Role:	PI	Co-I	Res. Assoc.	Co-I	Co-I	Research tech
Researcher Identifier (ORCID ID):	https://orcid.org/0000-0001-9813-7184	https://orcid.org/0000-0002-0762-1833	https://orcid.org/0000-0003-2947-021X	https://orcid.org/0000-0003-4639-807X	https://orcid.org/0000-0003-4208-7362	https://orcid.org/0000-0001-9843-4736
Nearest person month worked:	9	7	12	1	1	12
Contribution to Project:	Dr. Igoucheva supervised all aspects of the study and performed FACS analyses of patient-derived samples	Dr. Alexeev was involved in all aspects of the Aims 1 and 2, including analysis of bandage-derived cells and T cell-mediated immunity	Dr. Huitema was involved in all aspects of the Aims 1 and 2, including analysis of bandage-derived cells and T cell-mediated immunity	Dr. Uitto provided clinical expertise of collected patient material and patient data assessment	Dr. Debes has provided expertise in leukocyte assessment of patient-derived samples and helped with characterization of leukocytic infiltrates and T cell involvement	Ms. Phillips was involved in studies related to leukocytic infiltrates, T cell-mediated immunity and maintenance of mouse colony for studies outlined in Aim 3as well as maintenance of the laboratory
Funding Support:	No change	Internal support from Dr. Hatomi Sato Dr. Misue Terai Hasumi contract	No change	Two NIH R01 grants One pending NIH R01 subcontract DEBRA International	Two NIH R01 grants	No change

No other organizations were involved as partners.

10. SPECIAL REPORTING REQUIREMENTS

Nothing to report

11. APPENDIECIES

Nothing to report